

Comparison of Fracture Response Of Preflawned Tubes Under Internal Static and Detonation Loading

Tong Wa Chao and Joseph E. Shepherd

California Institute of Technology

Graduate Aeronautical Laboratories

Pasadena, CA 91125

U.S.A.

February 9, 2004

Abstract

The role of loading rate and fluid properties in the fracture of piping under internal explosions is an important issue for designers and accident analysis. This was examined by fracture experiments on thin-walled and preflawned aluminum 6061-T6 tubes. The tubes were 1) statically loaded with oil, 2) statically loaded with nitrogen, and 3) dynamically loaded with gaseous detonations traveling at 2.4 km/s. The tubes were also instrumented with pressure transducers, crack detection gages, and strain gages. The experiments were controlled so that comparisons could be made on identical specimens. Fracture behavior was discussed along with fluid dynamics.

Keywords: pipe, tube, fracture, rupture, crack, detonation.

Introduction

This study is motivated by our interest in the analysis of pipe rupture in accidental explosions and the fracture-based design of explosion vessels. A key issue is the effect of loading rate on fracture threshold and fracture propagation. Fracture of a pipe due to an internal detonation wave also represents a particularly challenging type of fluid-structure interaction that has been relatively unexplored. Tubes under internal static loading were studied extensively, especially for gas transmission pipelines. Examples of work done

on statically-loaded fracture of tubes include the pioneering analysis of through-wall cracked cylindrical shells [1] and full-scale gas transmission pipeline fracture experiments [2–4]. There are notable laboratory-scale pipe fracture experiments in conjunction with analytical and numerical efforts [5, 6]. There are also recent computational efforts [7] to simulate the fluid-structure-fracture interaction of a bursting pipe under initially static loading. The elastic response of shells to shock or detonation loading was examined by a number of researchers [8–12], but these studies did not involve fracture.

In our experiments, the flaw size and geometry, tube material, and nominal loading magnitude were kept constant. The loading rate and medium were varied. One case was static rupture by hydraulic oil; another, static rupture by gaseous nitrogen at room temperature; and the third, dynamic rupture by an internal gaseous detonation. The specimen ruptured under hydraulic oil loading had the least damage. Much more substantial damage, i.e., crack propagation and plastic deformation, was observed in the cases with nitrogen and detonation loading. The nitrogen loading caused a substantially larger fracture than the detonation although the peak loading pressure was similar.

Previous similar work was done at Caltech [13, 14] to investigate the structural response of unflawed cylindrical shells to internal shock and detonation loading. These analytical, numerical, and experimental studies demonstrated that the amplitude of the linear elastic strains are a function of both the pressure peak and the speed of the shock or detonation wave. Recent work at Caltech [15] studied the fracture behavior, strain response, and fracture surfaces of aluminum tubes under detonation loading with various flaw sizes.

Experimental Setup

Specimens

The specimens were thin-walled, seamless aluminum 6061-T6 tube. The surface notch was oriented axially, located in the middle of the tube length, and cut by a CNC machine using a jeweler’s slotting saw. The notch depth (0.56 mm), notch width (0.2 mm), tube size (0.89 mm in wall thickness, 41.28 mm in outer diameter, 0.610 m long), and notch length ($L = 25.4$ mm) were the same for all tests. Figure 1 shows the geometry of the flaw. $R_{saw} = 19$ mm is the radius of the jeweler’s slotting saw. The properties of Al6061-T6

are: $K_{Ic} = 30 \text{ MPa}\sqrt{\text{m}}$, $\rho = 2780 \text{ kg/m}^3$, $E = 69 \text{ GPa}$, and $\nu = 0.33$.

Detonation Tube Assembly

Figure 2 shows a schematic of the experimental setup for the detonation loading. The assembly was aligned and bolted to aluminum plates, which were bolted to a plywood table. The setup consisted of a thick-walled detonation tube connected to the specimen tube by a flange. The tubes were sealed at one end by a flange containing the spark plug, and the other end by a Mylar diaphragm. Inside the detonation tube, a spark first created a flame, which then transitioned to a detonation wave after being accelerated through a Shchelkin spiral. The detonation wave propagated into the specimen tube. The Mylar diaphragm is burst by the detonation so that the effects of a reflected shock wave were minimized. Pressure transducers mounted on the detonation tube measured the pressure profile and wave speeds.

For the gaseous nitrogen and hydraulic oil loading experiments, the specimen tube was connected to the same flanges used in the detonation experiments. The ends of the flanges were capped, threaded rods and nuts were used to counter the resulting hydrostatic axial force, and the assembly was fixed vertically rather than clamped down on a table.

Instrumentation

The velocity and pressure of the detonation wave were measured by PCB piezo-electric pressure transducers. The pressure transducers were mounted 0.406 m apart in the detonation tube.

Micro-Measurements strain gages and crack detection gages were bonded to the external surface of the tubes to measure circumferential strain and crack arrival times, respectively. Dow Corning 3145 RTV was used to protect the leads from premature destruction due to the blast wave. The Trig-Tek amplifiers that amplified the signals from the Wheatstone bridges had a bandwidth of 100 kHz.

In the detonation experiment, the spark and data acquisition system was triggered by a Stanford Research Systems digital pulse generator. The pressure traces, strain history, and crack arrival times were digitized with Tektronix oscilloscopes. The detonation experiment was recorded at a rate of 2.5 megasample per second, while the gaseous nitrogen and hydraulic oil experiments were recorded at a rate of 1 megasample

per second. The data were transferred into a computer through a LabVIEW program.

In the gaseous nitrogen and hydraulic oil experiments, one of the crack detection gages was placed close to the surface notch tip to trigger the data acquisition system. The pressure was recorded with an Omega PX4100-3KGV pressure transducer attached to one of the endcaps.

In the gaseous nitrogen experiment, nitrogen was supplied to the tube assembly from a liquid nitrogen tank via a pressure regulator and an electro-pneumatic valve. The pressure was slowly increased by turning a lever on the regulator. Upon rupture, the electro-pneumatic valve was closed by a manual switch.

In the hydraulic oil experiment, an SFX PowerTeam handpump was used to pressurize the tube assembly with SFX PowerTeam no. 9638 hydraulic oil.

Results and Discussion

Pressure Loading

For the detonation experiment, the mixture was stoichiometric ethylene-oxygen ($C_2H_4+3O_2$) at an initial pressure of 1.8 atm and room temperature. The pressure peak recorded by the pressure transducer is not reliable due to noise, the three-dimensional structure of the detonation wave front, and the finite size of the pressure transducer. For this reason, computed values of the Chapman-Jouguet (CJ) pressure were used to characterize the detonation. The calculated [16] CJ pressure and wave speed are 6.2 MPa and 2390 m/s. The detonation pressure history recorded on the pressure transducer closest to the flange is shown in Fig. 3. This is a typical gaseous detonation pressure trace with the initial CJ point (around 0.6 ms) coinciding with the shock front, immediately followed by a Taylor expansion wave. After the end of the Taylor expansion, there is a short plateau (1.2 to 1.6 ms) followed by the expansion wave that came from the rupture and the open end of the tube. The detonation wave speeds were measured just before entering the specimen tube and are typically within 5% of the computed values.

The burst pressures of the gaseous nitrogen experiment (5.5 MPa) and hydraulic oil experiment (6.0 MPa, see Fig. 3) were slightly lower than the CJ pressure of the detonation experiment. However, loading and unloading rates were quite different in the three cases. The pressure was increased very slowly in the static

tests and the loading rate was zero for all practical purposes in the nitrogen and hydraulic oil experiments. The pressure transducer used in the nitrogen and hydraulic oil experiments was too slow (response time of 10 ms) to capture the initial fast pressure transients during rupture (the original intention being only to capture the burst pressure). However, one can still get a rough idea of the depressurization rate. In the hydraulic experiment, it took about 15 ms to drop to about 3 MPa, while in the nitrogen experiment, it took as long as about 25 ms. In the detonation experiment, the loading is essentially complete after a few μ s, and the unloading occurs in two stages. Immediately following the detonation, it took only about 0.4 ms for pressure to drop from 6 MPa to 2 MPa and then a slower decay occurs over the next 5 ms. Note that these three pressure traces were recorded at different locations with very different gages so that the comparison is only qualitative.

Fracture Behavior as a Function of Loading

As can be seen in the post-test specimens in Fig. 4 (hydraulic oil), Fig. 5 (detonation), and Fig. 6 (gaseous nitrogen), the fracture behavior is a strong function of the applied loading.

In Fig. 5, the detonation wave traveled from left to right. As the wave propagated past the surface notch, the hoop stress opened the notch into a through-wall crack. Two crack fronts then propagated—one in the forward direction (i.e., same direction as the detonation wave) and one in the backward direction (i.e., in the opposite direction of the detonation wave). We will refer to these two crack fronts simply as the “forward” and “backward” cracks. Both the forward and backward cracks propagated straight for some distance, then turned, ran helically around the tube, and were arrested.

Under initially static gaseous loading with nitrogen, the cracks ran straight and did not arrest until they propagated to the supports (Fig. 6). Both cracks began to turn as they approached the supports.

In the experiment with hydraulic oil, the cracks were arrested almost immediately after they left the notch (Fig. 4). The cracks were so short that they did not run past enough crack detection gages for crack arrival time measurements. This behavior is relatively benign and in stark contrast to the extensive fractures observed with the static nitrogen or detonation tests. These observations support the standard practice [17] of hydrostatic pressure testing using liquids as opposed to pneumatic testing using gases.

Fractographs

Light microscope pictures of fracture surfaces were taken and some of these are shown for detonation and nitrogen experiments in Figs. 5 and 6, respectively. The magnification was 30X with a Leica GZ4 light microscope which was coupled to a Nikon Coolpix 990 digital camera. The natural scale in these photos is the wall thickness of the tubes, which is 0.89 mm.

Two types of fractographs can be discerned in the detonation experiment shown in Fig. 5. Both the forward and backward cracks first propagated straight for some distance, turned helically, and were arrested. Arrows next to the fractographs indicate the direction of propagation for the detonation waves and the cracks. The approximate locations on the tube where these fractographs were taken and the location of the initial notch are also shown.

The first type is shown in Fig. 5 (a) and (b). These fracture surfaces are along the straight portion of the cracks. They are relatively rough because 1) they were caused by the predominantly mode-I (opening mode) fracture and 2) the specimen was ductile, being above its transition temperature. Since the wall was thin, the fracture surfaces were, in general, slanted at 45 degrees to the specimen's surfaces and were composed almost entirely of shear lips. This is generally known as the 'thickness effect' in fracture mechanics [18].

The second type, less frequently reported in the literature, is shown in Fig. 5 (e) and (f). These fracture surfaces are along the curved portion of the cracks. They are relatively smoother than the fracture surfaces of the straight portion of cracks. The cracks have turned helically along the tube, and the fracture was predominantly mode-III (tearing mode) due to the large outward dynamic motion of the flaps. On some fracture surfaces, shallow striations that are almost perpendicular to the crack path can be seen, such as those in Fig. 5 (e) and (f).

The fracture surfaces of the gaseous nitrogen experiment are less distinctive from one another because the fracture mode stayed the same throughout the course of crack propagation. Nonetheless, the fracture surfaces farther from the notch tend to be somewhat smoother than those near the notch.

Strain Response

Figure 7 show the strain response of the specimen tubes within one or two milliseconds of rupture. In the detonation and gaseous nitrogen experiments, the strain gages and crack gages were located at the straight portions of the propagating cracks. The average crack speeds calculated from arrival times between consecutive crack gages are plotted in Fig. 9. The strain rates ranged typically from 10^2 s^{-1} to 10^3 s^{-1} .

The initial hoop strain patterns of the gaseous nitrogen and hydraulic oil experiments are qualitatively similar. They are on different time scales, but the strain histories of corresponding gages in the two experiments are generally of the same shape. In both plots, all strains start near the burst pressure. The initial drop in strain results from both the depressurization of the fluid and the motion of the flaps of material created by the propagating crack. The flaps fold outward and are hinged about the crack front; this motion compresses the material ahead of the crack. This hinge effect causes a drop in strain at a distance ahead of the crack and is common in flat-plate mode-I fracture. Since SG2 and SG3 were closer to the notch, as the cracks ran by, the crack tip stress concentrations along with the significant residual internal pressure caused sharp strain peaks. SG1 and SG4 were further from the notch, and one does not see such high strain peaks because the internal pressure had already been relieved quite significantly. Another point of interest is that although SG2 and SG3 in the hydraulic oil experiment are schematically symmetric about the notch, their signals look dissimilar because their actual locations were not symmetric about the notch.

“Static” Loading versus “Dynamic” Loading

The first important difference is the magnitude of the initial strain. The initial strain of the nitrogen and oil experiments is about 0.2%, equal to the static cylindrical shell prediction using the burst pressure. The magnitude of the first strain cycle (uncontaminated by stress concentrations because crack has not yet arrived) of the detonation experiment is about 0.3%, giving a dynamic amplification factor (ratio of dynamic strain to static prediction) of 1.5 using the CJ pressure. The traveling detonation load caused stresses and strains higher than static predictions. The steady-state [8] model predicts a dynamic amplification factor of 2 for the present situation. An extensive discussion of dynamic amplification factors as a function of detonation loading can be found in [14]. In that study, it was shown that the length of the tube and the location of

flanges can have a significant effect on the actual values of the amplification factor. If the amplification factor must be known exactly, then either detailed measurements or finite-element simulations are necessary.

The second important difference is the fatigue-like, oscillatory nature of the strain response caused by detonation load that is not observed in the static load cases. The first two or three cycles of strain that are shown by the strain gages on Fig. 7a show typical elastic strains of flexural waves excited by a detonation wave that traveled between the first two critical wave speeds of the structure. While the reader is referred to [14] and [15] for a more detailed discussion of detonation-induced flexural waves in tubes, several points are worth mentioning here. First, the strain front coincides with the detonation wave front. Second, the frequencies of the strains correspond closely to Tang's [8] theoretical steady-state frequency, which is 39 kHz for this tube. Third, since the flexural waves were dispersive and the detonation wave was traveling above the first critical wave speed, precursor waves at frequencies over 1 MHz would travel ahead of the strain signals associated with the main flexural wave. The reasons that they are invisible are that 1) they are of small amplitude compared to the main signal, and 2) the amplifiers, having a bandwidth of 100 kHz, attenuated the high frequency precursors.

The third important difference is that the loading and unloading have a preferred direction in the detonation case. The detonation propagates along the tube, creating a spatially-dependent stress field in the tube, sweeping over the notch, and setting up a flow field behind the wave. The crack initiation process will be asymmetric due to the interaction of the elastic waves created by the detonation passing over the notch and the strain field created by the fracture process itself. The expansion waves in the detonation interact with the flow field so that the subsequent stress field in the tube will be different upstream and downstream of the notch. This asymmetry will be reflected in an asymmetric fracture process. The results are the higher stresses and higher stress intensity factors associated with the forward crack. This is evidenced in the consistently higher crack speeds of the forward crack than those of the backward crack (Fig. 9a). The asymmetry was also demonstrated in a related study [15] on the fracture behavior as a function of initial flaw length using similar specimens. For short initial flaws, both the forward and backward cracks propagated helically without bifurcation. When the initial flaw size was increased, the forward crack bifurcated while a single backward crack propagated helically. This case was shown to be repeatable and was another indication of

a higher stress intensity factor at the forward crack tip due to the asymmetry of the loading. For very long initial flaws, both cracks bifurcated.

Crack Speeds

Crack speeds deduced from crack arrival times for the gaseous nitrogen loading fluctuated between 200 to 400 m/s, while those of detonation loading fluctuated between 170 to 250 m/s (Fig. 9). The error bars show upper and lower bounds. Crack speeds for hydraulic oil loading were not measured because the cracks were arrested before reaching the crack gage locations. From the measured crack speeds, it appears that the gaseous nitrogen loading provided a slightly larger crack driving force than the detonation loading. In the nitrogen case, the tube was prestressed everywhere when rupture occurred and the stress state decayed slowly in comparison to the fracture propagation time. A 200 m/s crack tip would propagate 0.3 m from the notch to the tube end in 1.5 ms, and the pressure decays a negligible amount during this time (Fig. 3). In the detonation case, only the portion of the tube behind the detonation wave was loaded and the pressure decays substantially during the time the crack tips propagate towards the ends of the tube (Fig. 3). Figure 8 shows plots of crack and detonation trajectories in $x-t$ diagrams. The detonation trajectories were predicted assuming that the fracture process did not affect the detonation velocity. The detonation wave speeds were obtained from the detonation front arrival times at the pressure transducers in the detonation tube, and then extrapolating the detonation trajectory into the specimen tube.

Fluid	c (m/s)	v (m^3/kg)	K_s (m^2/N)
Detonation Products	1300	0.24	1.4×10^{-7}
Nitrogen Gas	354	0.016	1.3×10^{-7}
Hydraulic Oil	1154	0.0011	8.3×10^{-10}

Table 1: Properties of the fluids used for loading. Detonation products are evaluated at CJ state. Nitrogen is evaluated at burst pressure of 5.5 MPa and room temperature. Since the sound speed of the hydraulic oil was not available from the manufacturer, it was measured in our laboratory.

Effect of Fluid Properties

The differences in observed fracture behavior are quite striking and most apparent when comparing the hydraulic oil loading with either of the two gas loading cases. This immediately suggests that the large difference in physical properties of gases and liquids is responsible for the differences in fracture behavior. The properties of greatest interest are specific volume v and sound speed c , which can be combined to form the isentropic compressibility

$$K_s \equiv -\frac{1}{v} \frac{\partial v}{\partial P} \Big|_s = \frac{v}{c^2}. \quad (1)$$

Values of these properties have been estimated for all three fluids used in present experiments and are given in Table 1. Inspection of these values indicates a two-order-of-magnitude difference between the gas and liquid compressibility. As shown below, the main consequence of this is that a much larger (three orders of magnitude) amount of energy can be stored at the same pressure in the compressed gases or detonation products than in the hydraulic oil. A secondary factor is that the crack speeds are comparable to the sound speeds in the nitrogen case but a factor of 5 lower than the sound speed in the detonation products.

We have identified three principle physical processes associated with the fluid-structure interaction that will influence the fracture process. First, the pressure will begin to drop in the tube once a thru-crack has developed and fluid begins venting out of the crack opening. This will reduce the pressure in the vicinity of the crack, lowering the hoop stress in the tube and reducing the crack driving force. Second, the local reduction in pressure due to the fluid venting will propagate through the fluid as an expansion wave, the head of this wave moving at the sound speed in the static fluid and with the sum of sound and flow velocities in the moving fluid. This will reduce hoop stress near or ahead of the crack tip, reducing the crack driving force. Third, the fluid does work through plastic deformation and acceleration of the “flaps” of material created by the fracture process. The amount of work that can be done is limited by the amount of energy initially stored in the fluid. This energy can be estimated from thermodynamic principles and compared to the elastic energy in the tube as well as the energy required to create new fracture surfaces. Brief explorations of each of these issues are given in the subsequent sections.

Venting

For a small (isentropic) change in specific volume Δv , the pressure drop ΔP is

$$\Delta P = \left. \frac{\Delta P}{\Delta v} \right|_s \Delta v = \left. \frac{\partial P}{\partial v} \right|_s \Delta v = -\frac{1}{K_s} \frac{\Delta v}{v}. \quad (2)$$

Inspection of the values in Table 1 indicates that the liquid will depressurize much more rapidly than the gases, causing the hoop stress near the original notch to rapidly decrease once the fluid starts to vent. For example, venting 0.5% of the original volume of the hydraulic oil is sufficient to drop the average pressure in the tube from 6 MPa to zero. On the other hand, venting a similar amount from the compressed nitrogen reduces the pressure only by 38 kPa, a factor of 10^2 less.

Expansion Waves

Expansion waves generated by the venting of fluid out of the crack opening will travel fastest in the detonation products and hydraulic oil and slowest in the nitrogen (Table 1). The situation is complex in the detonation case because the fluid is moving behind the detonation wave, creating a spatially nonuniform pressure field [14]. However, it is clear from the measured crack propagation speeds that the expansion waves travel 5 times faster than the crack tips and the detonation wave travels 10 times faster than the crack tips.

This means that the expansion waves travel faster than the crack tips in both the hydraulic oil and the detonation cases. This will result in a decrease in the hoop stress and decreasing crack driving force as the crack tip grows. This is one factor that causes the cracks in the detonation case to arrest early rather than propagate to the end of the tube as observed in the nitrogen case. In the nitrogen loading case, the expansion waves travel at a speed comparable to the crack tip. This suggests that the stress field ahead of the crack will be relatively unaffected by the expansion wave until the cracks arrive at the tube ends.

Energy Storage

Internal pressurization of the tubes is associated with stored energy due to the compressibility of the fluid and the elastic nature of the tube material. This stored energy will be converted into kinetic energy and

internal energy of the tube, fluid contents, and surrounding air. A notional energy balance for the process of fracture and tube rupture can be written as

$$\begin{aligned} \Delta U_{fluid}^{elastic} + \Delta U_{solid}^{elastic} = \Delta E_{fluid}^{K.E.} + \Delta E_{solid}^{K.E.} + \Delta E_{plastic} \\ + \Delta E_{fracture} + \Delta E_{dissipated} . \end{aligned} \quad (3)$$

A similar energy balance was considered by other researchers [5,19]. One of the main differences between the present study and the other two studies is the energy associated with the fluid. While the other two considered only the part of fluid energy which does work on the fracturing pipe by assuming a pressure decay profile and a flap displacement pattern, the present study considers maximum energy that is stored in the fluid from a thermodynamic point of view. The energy balance above represents a total energy approach and is different from those that aim to derive the crack driving force [18,20].

The terms on the left hand side account for the elastic strain energy stored relative to the reference configuration of the tube and fluid at atmospheric pressure. The terms on the right include kinetic energy of the tube, energy for large scale plastic deformation of the flaps, energy required for the fracture process, and dissipation due to heat transfer, etc., after rupture. Only a few of these terms will be estimated in this study.

Thermodynamic considerations can be used to provide upper bounds for stored energy in the fluid. For nitrogen, a perfect gas model $Pv = RT$ can be used and the stored energy estimated by considering isentropic expansion from the initial state (1) to the final state (2) at the pressure of the surrounding atmosphere

$$\Delta s = c_p \ln \frac{T_2}{T_1} - R \ln \frac{P_2}{P_1} = 0 , \quad c_p = \frac{\gamma R}{\gamma - 1} , \quad \frac{c_p}{c_v} = \gamma . \quad (4)$$

The compressibility varies inversely with pressure for an ideal gas

$$K_s = \frac{1}{\gamma P} \quad (5)$$

and this has to be taken into account when computing the stored energy for a gas. The simplest way to do

that is to use the first law of thermodynamics and evaluate the work done as the change in internal energy during the expansion from state 2 to 1

$$\Delta u = c_v(T_1 - T_2) , \quad (6)$$

with T_2 computed from Eq. (4). The energy change per unit mass during isentropic expansion of gaseous nitrogen is then

$$\Delta u_{nitrogen}^{elastic} = \frac{P_1 v_1}{\gamma - 1} \left[1 - \left(\frac{P_2}{P_1} \right)^{\frac{\gamma-1}{\gamma}} \right] . \quad (7)$$

A similar computation can be carried out for the high-pressure, hot gases behind the detonation wave, taking into account the kinetic energy in the products [21].

The stored energy in the hydraulic oil can be computed from the first law of thermodynamics to be

$$\Delta u_{oil}^{elastic} = \int_{v_1}^{v_2} P dv . \quad (8)$$

Since the volume change of the liquid is quite small for the pressures we are considering, it is easier to work with the pressure and write this as

$$\Delta u_{oil}^{elastic} = - \int_{P_1}^{P_2} v K_s P dP . \quad (9)$$

This can be simplified by assuming that the compressibility is constant so that by using the definition of K_s (Eq. (1)) and integrating to obtain the volume dependence on pressure

$$v = v_1 \exp(-K_s(P - P_1)) \quad (10)$$

Expanding in powers of the argument, we have

$$v \approx v_1(1 - K_s(P - P_1) + \mathcal{O}(K_s(P - P_1))^2) . \quad (11)$$

Retaining only the first term in this expansion, we can carry out the integration in Eq. (9) to obtain

$$\Delta u_{oil}^{elastic} \approx v_1 K_s \left(\frac{P_1^2 - P_2^2}{2} \right). \quad (12)$$

For comparison, it is better to work on a unit volume basis since the tubes contain a fixed volume of fluid.

For the gaseous nitrogen, this will be

$$\frac{\Delta U_{nitrogen}^{elastic}}{V} = \frac{P_1}{\gamma - 1} \left[1 - \left(\frac{P_2}{P_1} \right)^{\frac{\gamma-1}{\gamma}} \right] = 10 \text{ MJ/m}^3. \quad (13)$$

The Fickett-Jacobs thermodynamic cycle computation [21, 22] for $\text{C}_2\text{H}_4 + 3\text{O}_2$ detonation products yields

$$\frac{\Delta U_{detonation}^{elastic}}{V} = 5.1 \text{ MJ/m}^3. \quad (14)$$

For the hydraulic oil, this will be

$$\frac{\Delta U_{oil}^{elastic}}{V} \approx K_s \left(\frac{P_1^2 - P_2^2}{2} \right) = 15 \text{ kJ/m}^3. \quad (15)$$

In these calculations, it was assumed that $\gamma = 1.4$, $P_1 = 6 \text{ MPa}$, and $P_2 = 0.1 \text{ MPa}$. The energy stored in the gaseous nitrogen per unit volume is 10^3 times larger than that of the oil.

The elastic energy stored in the tube can be estimated by assuming that the extensions were all in the radial direction. This is a reasonable approximation for most of the tube since the ends were a slip-fit into the flanges, and the pressure on the endplates was balanced by threaded rods. If the hoop stress was the only principal stress, the elastic energy stored per unit volume in the solid before rupture is

$$\frac{1}{2} \sigma \epsilon = \frac{\Delta P^2 R^2}{2Eh^2}, \quad (16)$$

where $\Delta P = P_1 - P_2$. The rate at which the tube's elastic energy is released during fracture requires an analysis based on the equations of motion and computation of the energy flux into the crack tip. Lacking this, as a first estimate, we will assume that all the elastic energy in a ring of material with volume ($2\pi R h \Delta a$)

behind the crack tip is released during crack propagation. On this basis, the rate of elastic energy released per unit crack advance is

$$\frac{\Delta U_{solid}^{elastic}}{\Delta a} \approx \frac{\Delta P^2 R^2}{2Eh^2} (2\pi Rh) = \frac{\pi \Delta P^2 R^3}{Eh} = 16 \text{ J/m} \quad (17)$$

for $\Delta P = 6 \text{ MPa}$. From a fracture mechanics point of view [23], only a fraction of this energy will be used to create fracture surface because there are many other mechanisms for absorbing the stored energy in the fluid and tube. The energy requirement related to crack resistance (per unit crack advance) is

$$\frac{\Delta E_{fracture}}{\Delta a} \geq hG_c \quad (18)$$

where G_c is the fracture propagation toughness. Physically, this means that for fracture to occur, the rate of energy flow into the crack tip must be equal to or greater than the fracture propagation toughness. Although G_c was not measured for this study, it can be estimated [23] from the mode-I critical stress intensity of Al6061-T6

$$hG_c \approx h \frac{K_{Ic}^2}{E} = 12 \text{ J/m} . \quad (19)$$

The energy approximations above are summarized in Table 2. The energy stored in the fluid has been converted to energy per unit tube length to allow a more meaningful comparison with the elastic energy and fracture energy. It is clear that from energy considerations, the cracks were significantly shorter for oil loading than nitrogen loading because for the nearly incompressible liquid, a modest amount of stored energy was available to be converted to energy for driving a crack. For the very compressible gases, the stored energy was much larger, by a factor of 10^3 , and ample energy was available to create fracture surfaces.

Conclusion

The differences in the rupture behavior were examined in terms of the physical parameters of the fluids and their influence on the physical processes involved in the rupture event. The key role of fluid compressibility

Energy	Det. (J/m)	N ₂ (J/m)	Oil (J/m)
Fluid	6.9×10^3	13×10^3	20
Solid	16	16	16
Fracture	12	12	12

Table 2: Fluid energy stored per unit tube length compared to elastic solid energy release per unit crack advance and fracture energy expenditure per unit crack advance.

was highlighted. The striking difference between the results of tests with hydraulic oil and high-pressure gases can be explained in terms of stored energy in the fluid relative to the energy required for fracture surface generation. The initial stress state was an important factor in comparing the nitrogen and detonation cases. A secondary role of sound speed in determining expansion wave propagation was identified as probably being responsible for the observed differences between nitrogen and detonation products. Fluid compressibility is also a significant factor in the venting process that determines the pressure history once the crack begins to open.

Acknowledgments

The authors thank W. G. Knauss and G. Ravichandran for their helpful discussions and additionally thank Prof. Knauss for the loan of the hydraulic pump and hose. Our thanks also go to A. J. Rosakis and D. D. Anderson for lending us the circuit for conditioning crack detection gage signals. This research was sponsored in part through the Office of Naval Research (ONR) contract N00014-99-1-0744 and by the US DOE through the Caltech ASCI project.

Nomenclature

E	Young's modulus	N/m^2
G_c	fracture propagation toughness	J/m^2
K_{Ic}	mode-I critical stress intensity	$\text{MPa}\sqrt{\text{m}}$
K_s	isentropic compressibility	m^2/N
L	initial notch length	m
P	pressure	N/m^2
R	gas constant	$\text{J}/(\text{kg K})$
V	volume	m^3
$2a$	initial notch length	m
c	sound speed	m/s
c_p	specific heat at constant pressure	$\text{J}/(\text{kg K})$
c_v	specific heat at constant volume	$\text{J}/(\text{kg K})$
d	initial notch depth	m
h	shell thickness	m
s	specific entropy	$\text{J}/(\text{kg K})$
u	elastic energy per unit mass	J/kg
v	specific volume	m^3/kg
ΔE	energy per unit mass	J/kg
ΔU	elastic energy	J
γ	ratio of specific heats	
ν	Poisson's ratio	
ρ	density	kg/m^3

References

- [1] Folias, E. S., 1965. "A finite crack in a pressurized cylindrical shell". *International Journal of Fracture Mechanics*, **1**, pp. 104–113.

- [2] Maxey, W. A., Kiefner, J. F., Eiber, R. J., and Duffy, A. R., 1971. “Ductile fracture initiation, propagation, and arrest in cylindrical vessels”. In ASTM STP 514, Fracture Toughness, Proceedings of the 1971 National Symposium on Fracture Mechanics PART II.
- [3] Kiefner, J. F., Maxey, W. A., Eiber, R. J., and Duffy, A. R., 1973. “Failure stress levels of flaws in pressurized cylinders”. In ASTM STP 536, Progress in Flaw Growth and Fracture Toughness Testing, Proceedings of the 1972 National Symposium on Fracture Mechanics.
- [4] Ives, K., Shoemaker, A., and McCartney, R., 1974. “Pipe deformation during a running shear fracture in line pipe”. *Journal of Engineering Materials and Technology*, **96** (4) , pp. 309–317.
- [5] Emery, A. F., Kobayashi, A. S., Love, W. J., Place, B. W., Lee, C., and Chao, Y. H., 1986. “An experimental and analytical investigation of axial crack propagation in long pipes”. *Engineering Fracture Mechanics*, **23** (1) , pp. 215–226.
- [6] Kobayashi, A. S., Emery, A. F., Love, W. J., and Chao, Y. H., 1988. “Subsize experiments and numerical modeling of axial rupture of gas transmission lines”. *Journal of Pressure Vessel Technology*, **110** , pp. 155–160.
- [7] Zhuang, Z., and O’Donoghue, P., 2000. “Determination of material fracture toughness by a computational/experimental approach for rapid crack propagation in PE pipe”. *International Journal of Fracture*, **101** (3) , pp. 251–268.
- [8] Tang, S., 1965. “Dynamic response of a tube under moving pressure”. In Proceedings of the American Society of Civil Engineers, vol. 5, Engineering Mechanics Division, pp. 97–122.
- [9] Reismann, H., 1965. “Response of a pre-stressed cylindrical shell to moving pressure load”. In Eighth Midwest Mechanics Conference, S. Ostrach and R. Scanlon, Eds., Pergamon Press, pp. 349–363.
- [10] de Malherbe, M., Wing, R., Laderman, A., and Oppenheim, A., 1966. “Response of a cylindrical shell to internal blast loading”. *Journal of Mechanical Engineering Science*, **8** (1) , pp. 91–98.
- [11] Simkins, T., 1987. Resonance of flexural waves in gun tubes. Tech. Rep. ARCCB–TR–87008, US Army Armament Research, Development and Engineering Center, Watervliet, N.Y. 12189–4050, July.

- [12] Thomas, G., 2002. “The response of pipes and supports generated by gaseous detonations”. *Journal of Pressure Vessel Technology*, **124** , pp. 66–73.
- [13] Beltman, W., Burcsu, E., Shepherd, J., and Zuhail, L., 1999. “The structural response of cylindrical shells to internal shock loading”. *Journal of Pressure Vessel Technology*, **121** , pp. 315–322.
- [14] Beltman, W., and Shepherd, J., 2002. “Linear elastic response of tubes to internal detonation loading”. *Journal of Sound and Vibration*, **252** (4) , pp. 617–655.
- [15] Chao, T. W., and Shepherd, J. E., 2002. “Fracture response of externally-flawed cylindrical shells to internal gaseous detonation loading”. In ASME Pressure Vessels and Piping Conference, Emerging Technologies in Fluids, Structures, and Fluid-Structure Interactions, PVP Vol. 446-2, M. Fisher and A. Holdo, Eds., ASME, pp. 85–98.
- [16] Reynolds, W., 1986. The element potential method for chemical equilibrium analysis: implementation in the interactive program STANJAN. Tech. rep., Mechanical Engineering Department, Stanford University.
- [17] ASME, 2000. *ASME Boiler and Pressure Vessel Code - An International Code*. The American Society of Mechanical Engineers, New York, NY. Section VIII, Div. 1 (Part UG-100), Div. 2 (Article T-4).
- [18] Kanninen, M. F., and Popelar, C. H., 1985. *Advanced Fracture Mechanics*. Oxford University Press, New York.
- [19] Poynton, W. A., Shannon, R. W. E., and Fearnough, G. D., 1974. “The design and application of shear fracture propagation studies”. *Journal of Engineering Materials and Technology*, **96** (4) , pp. 323–329.
- [20] Freund, L. B., 1998. *Dynamic Fracture Mechanics*. Cambridge University Press.
- [21] Fickett, W., and Davis, W. C., 2001. *Detonation: Theory and Experiment*. Dover.
- [22] Wintenberger, E., 2003. Private communication.
- [23] Broek, D., 1997. *Elementary Engineering Fracture Mechanics*, fourth revised ed. Kluwer academic publishers.

List of Figures

1	Flaw geometry.	21
2	Tube assembly schematic for detonation experiment.	22
3	Pressure traces for detonation (a), nitrogen (b), and oil (c) loading.	23
4	Post-test specimen of hydraulic experiment.	24
5	Fractographs, post-test specimen, and crack path schematic for a tube fractured under detonation loading.	25
6	Fractographs, post-test specimen, and crack path schematic for a tube fractured under gaseous nitrogen loading.	26
7	Hoop strains for detonation (a), gaseous nitrogen (b), and oil (c) cases. The initial strain is zero in all cases for the detonation case. For the static cases, strains begin at values corresponding to burst. Zero strains are indicated by dashed lines.	27
8	Representation of the $x-t$ diagram of detonation (a) and gaseous nitrogen (b) experiments.	28
9	Crack speeds for a tube under detonation (a) and gaseous nitrogen (b) loading.	29

List of Tables

1	Properties of the fluids used for loading. Detonation products are evaluated at CJ state. Nitrogen is evaluated at burst pressure of 5.5 MPa and room temperature. Since the sound speed of the hydraulic oil was not available from the manufacturer, it was measured in our laboratory.	9
2	Fluid energy stored per unit tube length compared to elastic solid energy release per unit crack advance and fracture energy expenditure per unit crack advance.	16

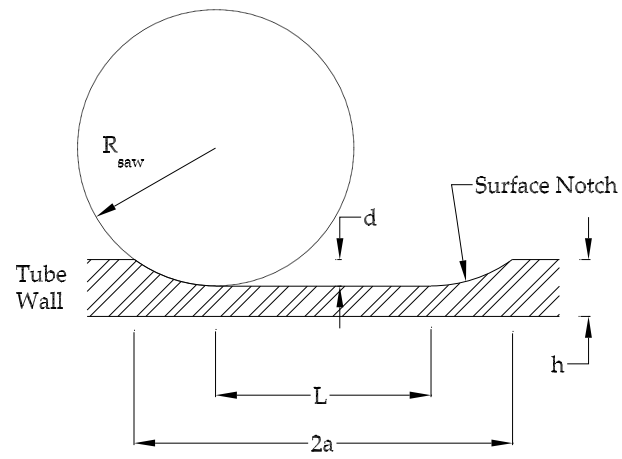


Figure 1: Flaw geometry.

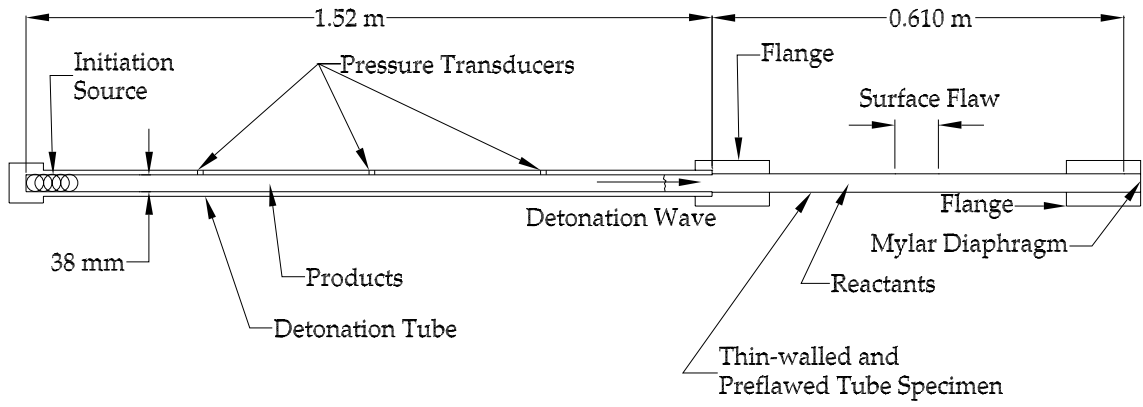


Figure 2: Tube assembly schematic for detonation experiment.

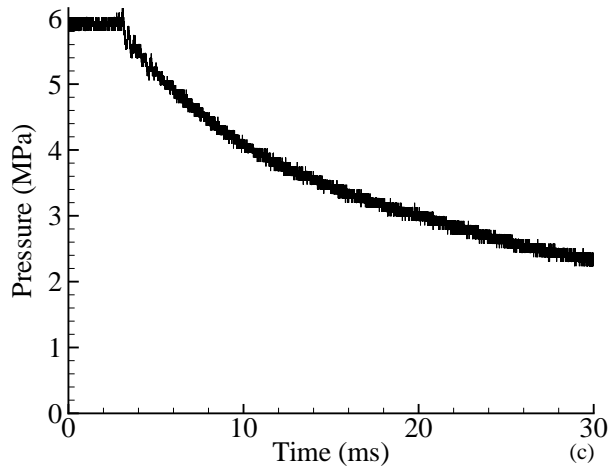
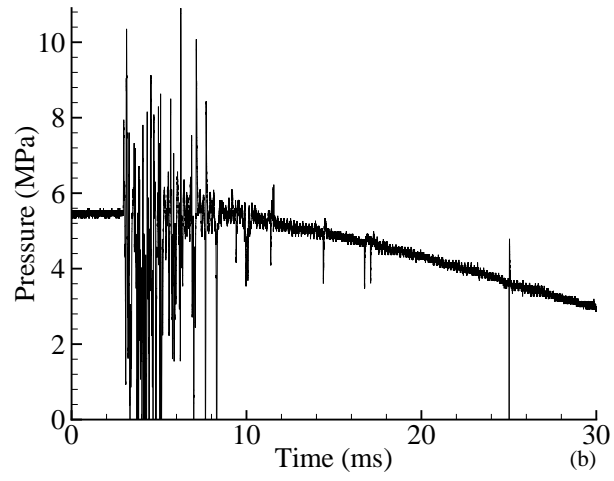
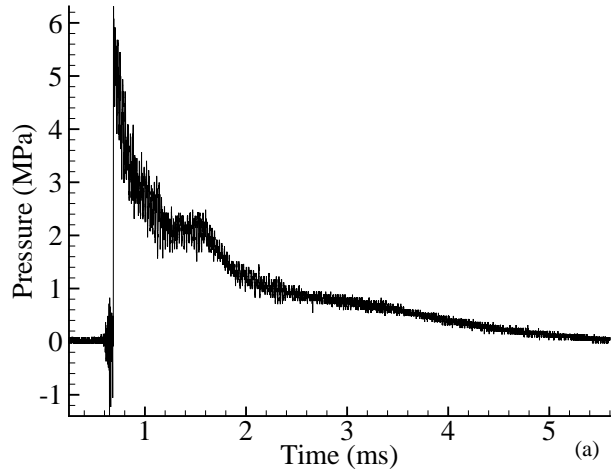


Figure 3: Pressure traces for detonation (a), nitrogen (b), and oil (c) loading.

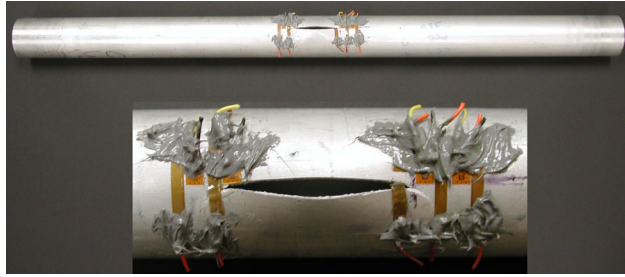


Figure 4: Post-test specimen of hydraulic experiment.

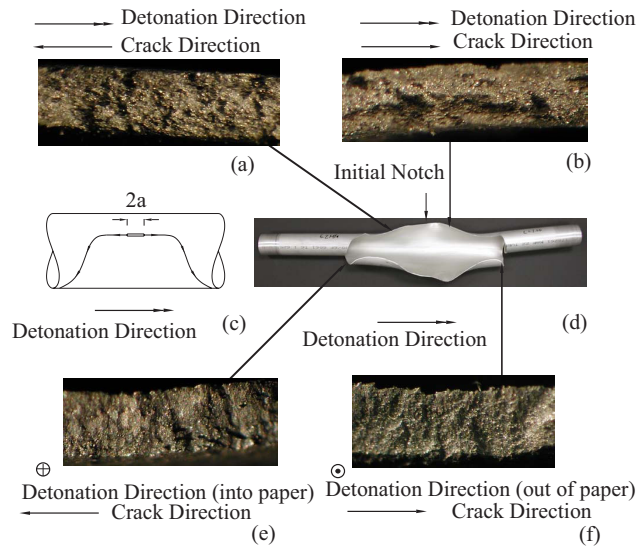


Figure 5: Fractographs, post-test specimen, and crack path schematic for a tube fractured under detonation loading.

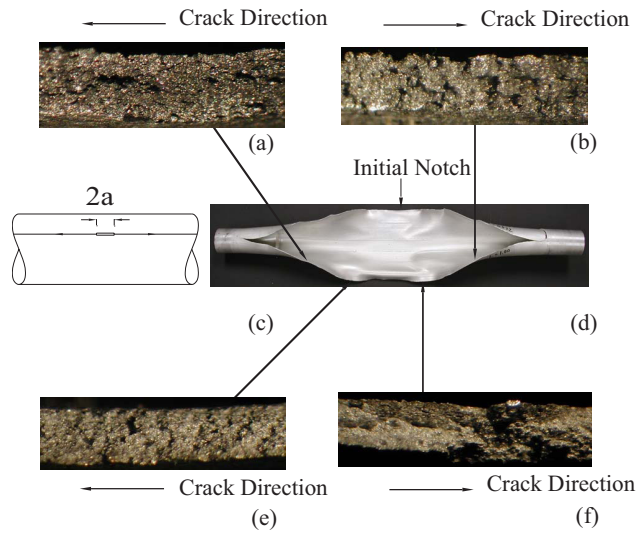


Figure 6: Fractographs, post-test specimen, and crack path schematic for a tube fractured under gaseous nitrogen loading.

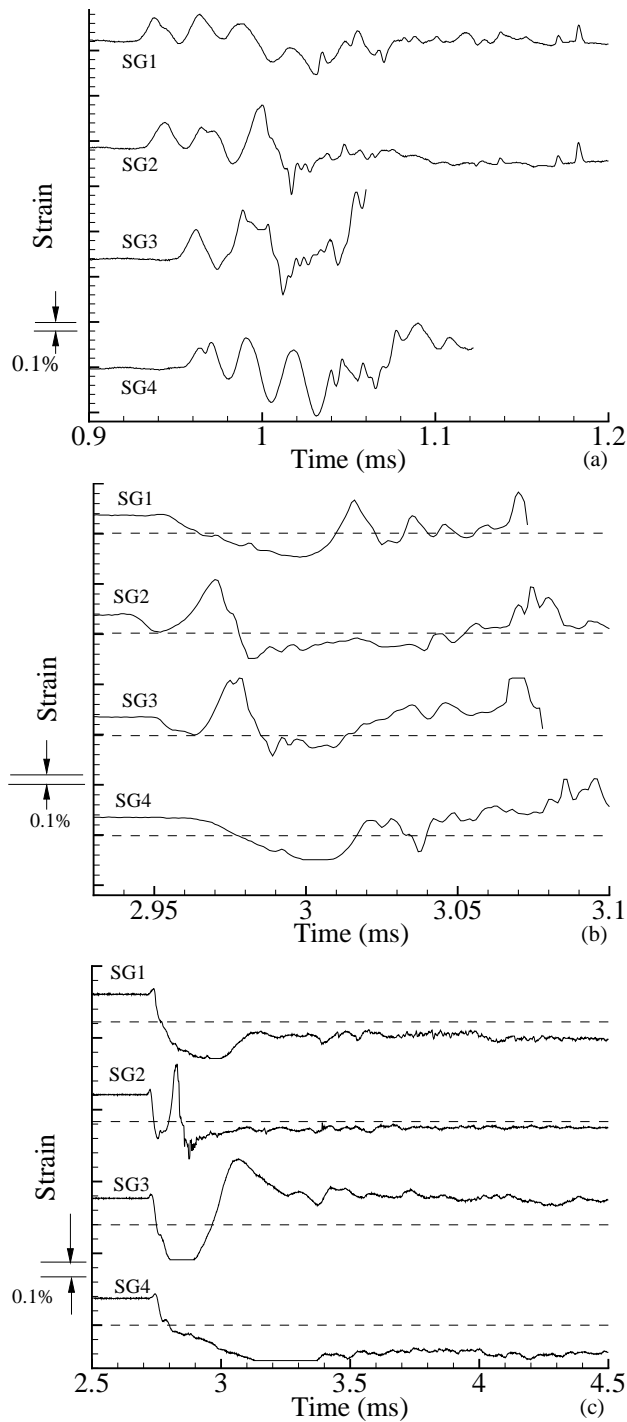


Figure 7: Hoop strains for detonation (a), gaseous nitrogen (b), and oil (c) cases. The initial strain is zero in all cases for the detonation case. For the static cases, strains begin at values corresponding to burst. Zero strains are indicated by dashed lines.

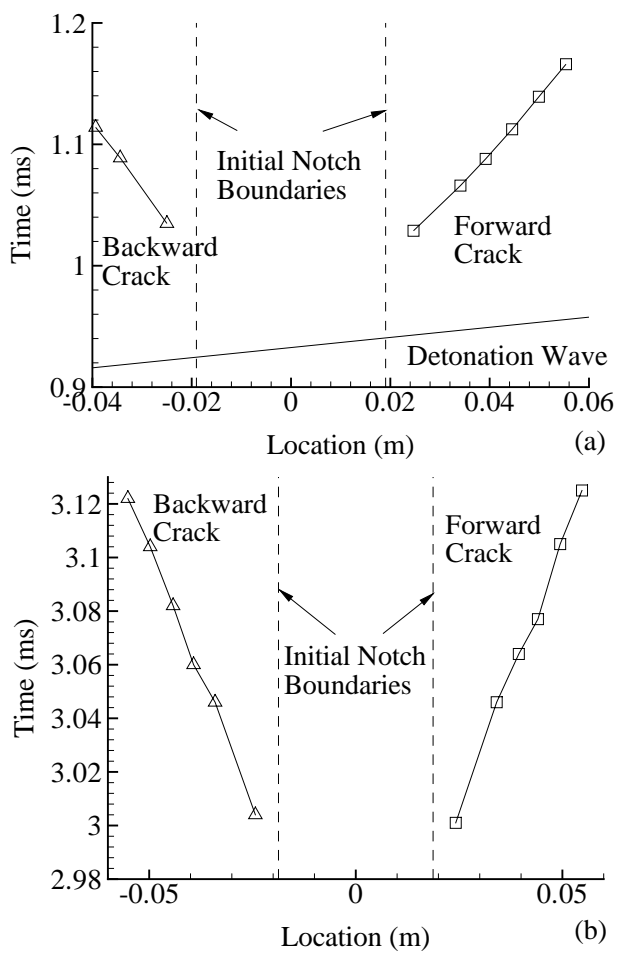


Figure 8: Representation of the $x-t$ diagram of detonation (a) and gaseous nitrogen (b) experiments.

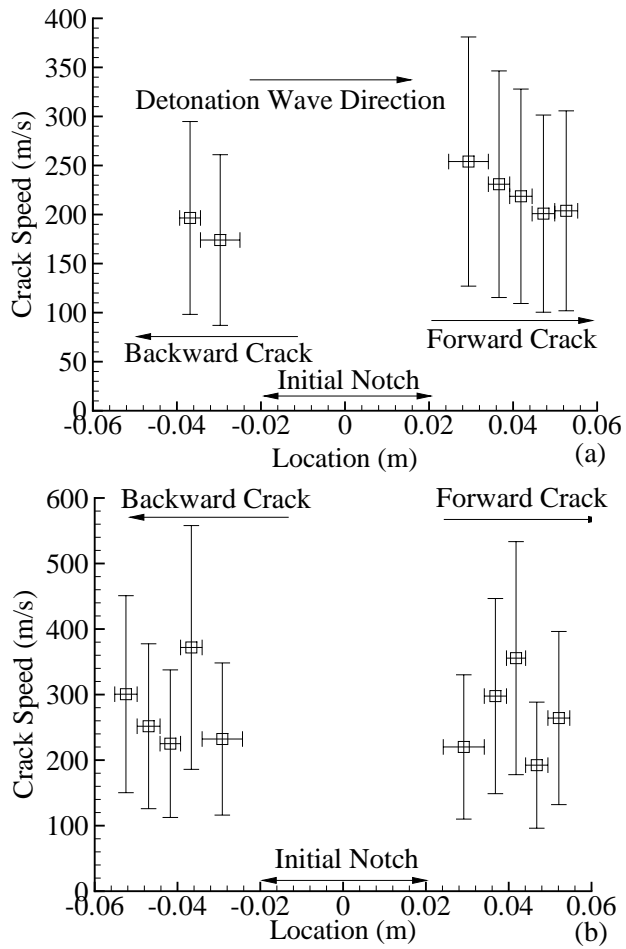


Figure 9: Crack speeds for a tube under detonation (a) and gaseous nitrogen (b) loading.